J. Fluid Mech. (1979), *vol.* 95, *part* 1, *pp.* 119–139
Printed in Great Britain

Numerical solution of the exact equations for capillary–gravity waves

By LEONARD W. SCHWARTZ
AND JEAN-MARC VANDEN-BROECK†
Department of Applied Mathematics, University of Adelaide, S. Australia

(Received 15 September 1978 and in revised form 20 February 1979)

A numerical method is presented for the computation of two-dimensional periodic progressive surface waves propagating under the combined influence of gravity and surface tension. The dynamic boundary equation is used in its exact nonlinear form. The procedure involves a boundary-integral formulation coupled with a Newtonian iteration. Solutions of high accuracy can be achieved over much of the range of wavelengths and heights including limiting waves. A number of different continuous families of solutions have been produced, all of which ultimately exhibit closed bubbles at their troughs. The so-called critical wavelengths are less important than have been previously assumed; the number of possible wave forms does increase with increasing wavelength, however.

1. Introduction

This paper deals with the computation of finite amplitude waves whose form is symmetric and that propagate without change of form on a deep liquid. We assume the liquid to be inviscid and incompressible and the flow to be irrotational. The free surface condition, including the effects of capillarity, is used in its exact nonlinear form.

A very substantial literature exists in the field of periodic surface waves of permanent form. The classical work of Stokes (1849, 1880) postulated the existence of periodic waves where gravity is the only restoring force and presented a perturbation procedure for their calculation as a series in a parameter equivalent to the wave steepness. Proofs of the convergence of this series for finite steepness, hence the mathematical existence of permanent waves, were devised by Nekrasov (1921) and Levi-Civita (1925). More recently, Krasovskii (1960) and others have produced elegant function-analytic proofs establishing the existence of steady gravity waves with surface slopes as great as 30 degrees to the horizontal.

Longuet-Higgins & Fox (1977), by developing a local solution valid near the crest of the almost-highest wave, have shown that the maximum surface elevation can exceed 30 degrees. An alternative existence proof has been produced very recently by Keady & Norbury (1978) which includes these extreme cases as well.

Numerical results of high accuracy for all but the steepest waves in water of both infinite and finite depth were produced by Schwartz (1972, 1974) who extended Stokes' series to high order by computer and then recast these polynomials as rational

† Present address: Courant Institute of Mathematical Sciences, New York University, New York.

0022–1120/79/4315–7620 $02.00

fractions. Additionally, a battery of 'series improvement' techniques, as introduced into the fluid mechanics literature by Van Dyke (1970), was employed to reveal details of the analytic structure of the solution. This semi-analytic approach was further refined by Longuet-Higgins (1975) and Cokelet (1977). A number of purely numerical attacks have been made on this nonlinear problem; among the most successful have been the work of Yamada & Shiotani (1968) and Sasaki & Murakami (1973).

The equivalent problem for pure capillary waves in deep water has been resolved completely by Crapper (1957) who produced an exact closed-form solution in terms of elementary functions. Closed-form solutions have recently been found for finite depth cases by Kinnersley (1976), a result anticipated by Crapper.

The combined gravity–capillarity problem would appear to be more formidable. Approximate solutions were published long ago by Harrison (1909), Wilton (1915) and Kamesvara Rav (1920). In each case, the surface profile was sought as a Fourier series in the horizontal co-ordinate or, equivalently, the velocity potential with coefficients that are power series in the wave amplitude. These perturbation expansions invoked 'Stokes' hypothesis' that the nth Fourier coefficient is nth order in the amplitude. While entirely satisfactory for the gravity wave, the use of this hypothesis in the general problem resulted in infinite values for certain of the series coefficients when the dimensionless capillary number κ is taken to be the reciprocal of a positive integer. Harrison noted this difficulty for $\kappa = \frac{1}{2}$ and Wilton, who carried the expansion to fifth order in the steepness, gave the general result. For the particular case of $\kappa = \frac{1}{2}$, Wilton, by revoking Stokes' hypothesis and re-ordering the terms in his series, was able to find *two* solutions, each of which he computed to third order. While, for $\kappa > \frac{1}{2}$, the small-amplitude profile was purely sinusoidal, Wilton's profiles for the critical value each exhibited a dimple, at the crest and at the trough, respectively. More recently, Pierson & Fife (1961) used the method of strained co-ordinates to extend the applicability of Wilton's two profiles to a neighbourhood of $\kappa = \frac{1}{2}$. Nayfeh (1970) produced an expansion valid near $\kappa = \frac{1}{3}$ using a multiple-scales technique. He found three different multi-dimpled profiles, none of which was equivalent to Wilton's. These first two critical values of κ correspond to wavelengths of 2·44 and 2·99 cm in deep water.

Additional interest in periodic waves with combined gravity and capillary forces derives from their applicability to two important, and related, problems. A significant contribution to the theory of wave-breaking was made by Longuet-Higgins (1963) who proposed a mechanism for the nonlinear transfer of energy from very steep gravity waves to capillary ripples that 'ride' on the forward faces of the long waves. This work was continued by Crapper (1970) who made use of his exact solution as well as the 'averaged Lagrangian' technique introduced by Whitham. Moreover, capillary–gravity waves near the critical wavelengths are an important example of resonant wave interactions. Recent work includes that of McGoldrick (1970*a*, *b*) and Nayfeh (1971).

In § 2 of the present paper we formulate the exact inviscid problem using the velocity potential and the stream function as independent variables. For convenience each fluid cycle is mapped conformally into the interior of the unit circle. The dependent variables are the co-ordinates of points on the free surface. They are related to one another by the dynamical free-surface condition and, since they are the real and imaginary parts of an analytic function, by the Hilbert formulae.

Details of the numerical procedure are given in § 3. We choose as unknowns a vector of surface ordinates. Numerical integrations of the principal-value boundary integral yield the corresponding horizontal co-ordinates. This trial solution is then substituted in the surface condition, resulting in an error vector which may be interpreted as a surface pressure distribution. This error vector is made uniformly small via a Newtonian iteration. The method is similar in philosophy, if not in detail, to the procedure used by Vanden-Broeck, Schwartz & Tuck (1978) to produce the gravity wave train behind barge-like, surface-piercing bodies.

Results of the calculations are presented in § 4. As a calibration, we compare with the exact results in the capillary limit and the effectively exact results for pure gravity waves. In the former case, 5-decimal-place accuracy can be easily achieved, up to the limiting trapped-bubble profile, with 40 to 50 surface points and a few iterations. Accuracy in the gravity limit is less good with equal point spacing; a simple redistribution of points so as to cluster them in the vicinity of the incipient sharp crest produces accurate results even for very steep waves. In fact a new local minimum of phase velocity for wave heights about 0·1 per cent short of the maximum is indicated. [This minimum, in fact an infinitude of local extremes, has recently been predicted analytically by Longuet-Higgins & Fox (1978).]

The bulk of § 4 is concerned with combined gravity–capillarity cases. Waves of maximum height have been computed for a number of values of κ. In all cases these waves are topologically limited by trapped bubbles rather than singularity-limited. This is apparently true even for small κ, corresponding to rather long wavelengths. Many different solutions corresponding to waves of different type have been found. These waves evolve continuously with changes in κ or amplitude and can retain their individual identities even when passing through several of the so-called critical values. Four different types have been studied in detail, two of which correspond to the dimpled profiles of Wilton. Of these two, one is, in fact, the analytic continuation of Crapper's wave. For a small value of κ, we present a profile which may be interpreted as a train of ripples riding upon a nonlinear gravity wave. The data presented in this section were compiled from about 400 separate converged solutions but is still by no means exhaustive.

The concluding section attempts to view the solution in perspective and also includes a conjecture on the convergence of Wilton's series solution.

2. Mathematical formulation

We consider symmetrical two-dimensional periodic waves moving with constant speed c relative to an inertial frame on the surface of a fluid of infinite depth. Consider a second reference frame moving with a wave crest. With respect to this frame the motion is steady; the general direction of flow being from left to right. Assuming irrotational motion of an inviscid, incompressible fluid, the solution may be represented as an analytic function of the complex variable $z = x + iy$ within the fluid region. The dynamical condition on the free surface is the Bernoulli equation

$$\tfrac{1}{2}q_s \bar{q}_s + gy_s + T/\rho R_s = \tfrac{1}{2}c^2. \tag{2.1}$$

Here $q = u - iv$ is the complex velocity, the bar signifies conjugation, and the subscript s denotes surface values. T, the surface tension, is non-negative, and ρ is the constant

fluid density. The acceleration of gravity g acts in the negative y direction. The y axis is taken as a line of symmetry of a surface wave whose length is denoted by λ. R_s is the radius of curvature, counted positive when the centre of curvature lies on the fluid side of the free surface.

The choice of the Bernoulli constant in (2.1) fixes the origin of y at the mean surface elevation. Since

$$\int_0^\lambda q_s \bar{q}_s \, dx = \lambda c^2 \tag{2.2a}$$

and

$$\int_0^\lambda dx/R_s = 0, \tag{2.2b}$$

it follows that

$$\int_0^\lambda y_s dx = 0. \tag{2.2c}$$

The derivation of (2.2a) may be found in Wehausen & Laitone (1960, § 32). It is true only for the case of infinite depth; for flows in finite depth with a horizontal bottom, (2.2a) conflicts with the usual definition of wave velocity. Equation (2.2b) is a general property of smooth periodic curves.

Proceeding now to dimensionless variables, we choose the speed of a small-amplitude gravity wave in deep water $(g\lambda/2\pi)^{\frac{1}{2}}$ as reference velocity and $\lambda/2\pi$ as reference length. In addition following Wilton and using his notation we define the dimensionless capillary number

$$\kappa = 4\pi^2 T/\rho g \lambda^2, \tag{2.3}$$

and the wave-speed parameter

$$\mu = 2\pi c^2/g\lambda. \tag{2.4}$$

The surface condition may now be written as

$$\tfrac{1}{2} q_s \bar{q}_s + y_s + \kappa/R_s = \tfrac{1}{2}\mu \tag{2.5}$$

in non-dimensional form.

Following the method devised by Stokes (1880) for periodic gravity waves, we choose the complex potential

$$f = \phi + i\psi$$

as the independent variable and let the fluid region correspond to the half-plane $\psi \leqslant 0$. The unknown function may be considered to be the sum of a uniform flow of speed $\sqrt{\mu}$ and a perturbation; thus

$$z = \mu^{-\frac{1}{2}} f + z^*, \tag{2.6}$$

where z^* must vanish as $\psi \to -\infty$. The periodicity can conveniently be imposed by a further transformation of the independent variable

$$f = \phi + i\psi = i\mu^{\frac{1}{2}} \log \zeta, \tag{2.7}$$

where $\zeta = re^{i\theta}$, which maps each fluid cycle onto the interior of the unit circle in the ζ-plane. This transformation was first used for the gravity wave problem by Nekrasov (1921). Equation (2.6) now becomes

$$z(\zeta) = i \log \zeta + z^*(\zeta) \tag{2.8}$$

or, upon differentiating,

$$\zeta \frac{dz}{d\zeta} = i + \zeta \frac{dz^*}{d\zeta}. \tag{2.9}$$

We equate real and imaginary parts of (2.9) on the free surface, $\psi = 0$ or $r = 1$, to obtain

$$x'(\theta) = -1 + x^{*\prime}(\theta)$$

and

$$y'(\theta) = y^{*\prime}(\theta).$$

The starred variables have the periodicity property

$$\int_{-\pi}^{\pi} x^{*\prime}(\theta)\, d\theta = \int_{-\pi}^{\pi} y^{*\prime}(\theta)\, d\theta = 0$$

and $\zeta z^{*\prime}(\zeta)$ is regular for $|\zeta| < 1$; consequently $x^{*\prime}$ and $y^{*\prime}$ obey the Hilbert formulae (see, for example, Tricomi, 1957, p. 167) on the unit circle. Returning to the unstarred variables, we have

$$x'(\theta) = -1 + \frac{1}{2\pi} \int_{-\pi}^{\pi} \cot\left(\frac{\varphi - \theta}{2}\right) y'(\varphi)\, d\varphi, \tag{2.10}$$

where the Cauchy principal value of the integral is implied. Exploiting the bilateral symmetry of the wave form about $\theta = 0$, equation (2.10) may be rewritten as

$$x'(\theta) = -1 + \frac{1}{2\pi} \int_{0}^{\pi} y'(\varphi) \left[\cot\left(\frac{\varphi - \theta}{2}\right) + \cot\left(\frac{\varphi + \theta}{2}\right)\right] d\varphi. \tag{2.11}$$

The surface condition (2.5) can now be expressed in terms of the new variables. In general the complex velocity is given as

$$q = u - iv = \frac{df}{dz} = \frac{df/d\zeta}{dz/d\zeta} = \frac{i\sqrt{\mu}}{\zeta z_{\zeta}} \tag{2.12}$$

and, therefore, on $r = 1$, we obtain

$$q\bar{q} = \frac{\mu}{x'^2 + y'^2}.$$

The curvature may be written parametrically in terms of the functions $x(\theta)$ and $y(\theta)$ as

$$\frac{1}{R} = \frac{x'y'' - y'x''}{[x'^2 + y'^2]^{\frac{3}{2}}}.$$

The final form of the Bernoulli equation is now

$$\frac{y}{\mu} + \frac{1}{2}\left(\frac{1}{x'^2 + y'^2} - 1\right) + \frac{\kappa}{\mu}\left(\frac{x'y'' - y'x''}{[x'^2 + y'^2]^{\frac{3}{2}}}\right) = 0. \tag{2.13}$$

In addition to the parameters κ and μ, a given wave is characterized by a third parameter which is a measure of the wave steepness. We choose this non-dimensional number to be

$$\epsilon = \frac{y(0) - y(\pi)}{2\pi}, \tag{2.14}$$

i.e. the differential elevation of the free surface over half a wave cycle. Dimensional analysis implies that a functional relationship should exist among these three numbers:

$$\text{function } (\mu, \kappa, \epsilon) = 0. \tag{2.15}$$

We fix two of the three parameters in (2.15) and we seek two functions $x(\theta)$ and $y(\theta)$, $\theta \in [0, \pi]$, and a value for the third parameter that simultaneously satisfy (2.11)

and (2.13). In the present paper we fix κ and ϵ and find μ as part of the solution. We will subsequently demonstrate that, unless $\kappa = 0$, this system of equations has, in general, many continuous solutions.

3. The numerical procedure

We shall describe the principal numerical method used to obtain the results in § 4; an alternative procedure, differing somewhat in detail, was used for the computation of steep gravity waves.

The numerical solution of equation (2.13) subject to the condition (2.11) is accomplished by a finite-difference method. The domain of the independent variable $\theta \in [0, \pi]$ is subdivided into N equal intervals. A vector of $N+1$ unknowns is the set of surface ordinates bounding these intervals. Thus

$$y_i = y(\theta_i), \tag{3.1a}$$

where

$$\theta_i = \frac{i-1}{N}\pi, \quad i = 1, \ldots, N+1. \tag{3.1b}$$

The derivatives are approximated using centred 5-point difference formulas and the integration in (2.11) is done by Simpson's rule. This discretization involves a nominal relative error which is fourth order in the point spacing. The difference formulas need to be modified near the ends of the interval according to relations expressing the periodicity and assumed symmetry of the surface profile:

$$\left.\begin{aligned} y'(\theta) &= -y'(-\theta) = -y'(2\pi-\theta); \\ y''(\theta) &= y''(-\theta) = y''(2\pi-\theta); \\ \text{and} \quad x''(\theta) &= -x''(-\theta) = -x''(2\pi-\theta). \end{aligned}\right\} \tag{3.2}$$

The treatment of the Cauchy-principal-value integral follows standard lines. If we replace φ by θ_i and θ by θ_j in (2.11) and denote the integrand by g_{ij}, we obtain immediately

$$g_{ij} = y_i' \left[\cot\left(\frac{\theta_i - \theta_j}{2}\right) + \cot\left(\frac{\theta_i + \theta_j}{2}\right)\right], \tag{3.3a}$$

for $i \neq j$. When $i = j$ and $i \in [2, N]$ we define

$$g_{ii} = y_i' \cot\theta_i + \lim_{\epsilon \to 0} \frac{1}{2\epsilon} \int_{\theta_i - \epsilon}^{\theta_i + \epsilon} y'(\alpha) \cot\left(\frac{\alpha - \theta_i}{2}\right) d\alpha,$$

which, upon expanding the integrand about $\alpha = \theta_i$ and cancelling the singular term by symmetry, yields

$$g_{ii} = y_i' \cot\theta_i + 2y_i'', \quad i = 2, \ldots, N. \tag{3.3b}$$

A similar approach for the end points gives

$$g_{ii} = 4y_i'', \quad i = 1 \text{ or } N+1. \tag{3.3c}$$

By using the above formulas, equation (2.11) may be approximated by the linear relations

$$x_j' = -1 + \sum_{i=1}^{N+1} b_{ij} y_i, \quad j = 1, \ldots, N+1, \tag{3.4}$$

where the coefficients b_{ij} depend only upon N and the details of the differentiation and integration schemes.

We seek to satisfy (2.13) at the $N+1$ points on the surface. With a given discretization (2.13) is replaced by $N+1$ nonlinear algebraic equations which may be written symbolically as

$$f_k(y_1, \ldots, y_N, \mu) = 0, \quad k = 1, \ldots, N+1. \tag{3.5}$$

Here the number of unknowns has been reduced by one by introducing the wave-height parameter

$$y_{N+1} = y_1 - 2\pi\epsilon. \tag{3.6}$$

The system (3.5) is solved by a process of Newtonian iteration. Thus, if we have an approximate solution $y_1, \ldots, y_N, \mu$ that produces a residual error vector E_k on the right-hand side of (3.5), the first-order corrections $\delta y_1, \ldots, \delta y_N, \delta\mu$ are given by the solution to the system of linear equations

$$\begin{bmatrix} \frac{\partial f_1}{\partial y_1} & \cdots & \frac{\partial f_1}{\partial y_N} & \frac{\partial f_1}{\partial \mu} \\ \vdots & & & \vdots \\ \frac{\partial f_{N+1}}{\partial y_1} & \cdots & \frac{\partial f_{N+1}}{\partial y_N} & \frac{\partial f_{N+1}}{\partial \mu} \end{bmatrix} \begin{bmatrix} \delta y_1 \\ \vdots \\ \delta y_N \\ \delta\mu \end{bmatrix} = \begin{bmatrix} -E_1 \\ \vdots \\ -E_{N+1} \end{bmatrix}. \tag{3.7}$$

The coefficient matrix in (3.7) depends on the current values of the variables $y_1, \ldots, y_N, \mu$ as well as the parameters ϵ and κ and the details of the discretization. The residual error vector E_k is a direct measure of the accuracy with which the free-surface condition is satisfied, and in fact can be interpreted as the difference between the computed 'pressure' and the required zero level.

For most of the cases discussed below, the scheme was found to be quadratically convergent; three to five iterations were required to satisfy the algebraic equations with an error less than 10^{-12}. A standard linear equation package was used to solve the system (3.7). With $N = 40$, each iteration required about 1 s on a CDC CYBER 173 computer. Most of the computation time was spent in solving (3.7); consequently the total time required to produce a single converged solution was approximately proportional to N^3. It was usually sufficient to start the iteration with a cosine profile and with $\mu = 1 + \kappa$, the infinitesimal wave solution.

4. Discussion of results

(*a*) *Pure capillary and gravity waves*

Before proceeding to the general case where the restoring forces include both gravity and surface tension, it would seem desirable to determine the accuracy of the present method by comparing results with the known, deep-water, solutions for the two limiting cases.

In a most remarkable paper, Crapper (1957) presented an exact closed form solution for capillary waves of arbitrary amplitude. In particular, for the wave speed, he found the simple expression

$$\mu/\kappa = (1 + \tfrac{1}{4}\pi^2\epsilon^2)^{-\frac{1}{2}} \tag{4.1}$$

	μ/κ			
ϵ	$N = 30$	$N = 40$	$N = 50$	Exact
0	1·00000	1·00000	1·00000	1·00000
0·1	0·98789	0·98789	0·98789	0·98789
0·2	0·95402	0·95403	0·95403	0·95403
0·3	0·90459	0·90459	0·90459	0·90459
0·4	0·84675	0·84674	0·84674	0·84673
0·5	0·78648	0·78645	0·78644	0·78644
0·6	0·72780	0·72775	0·72774	0·72773
0·65	0·69981	0·69974	0·69973	0·69972
0·70	0·67295	0·67286	0·67283	0·67282
0·73	0·65749	0·65730	0·65726	0·65726

TABLE 1. Wave speed *versus* wave height for pure capillary waves.

using the present notation. As the wave steepness increases the troughs of the surface profile become narrower and the crests more broad. The limiting value of steepness, $\epsilon = 0{\cdot}730$, corresponds to a profile where the two sides of the trough meet one another, enclosing a pendant-shaped 'bubble of air'. While steeper waves may be calculated, they are topologically impossible since the free surface crosses itself. Because no singularities appear in or near the fluid region, the present numerical method might be expected to work well. Table 1 shows computed values of wave speed versus wave amplitude for N, the number of intervals in a half-wavelength, taken equal to 30, 40 and 50 respectively. The last column is Crapper's exact result (4.1). The numerical values were obtained using the capillary number κ equal to 10^6. For $N = 30$, the greatest error is about one part in 3000; this discrepancy decreases to one part in 10^5 for $N = 50$. The surface profiles, however, even with $N = 30$, are graphically indistinguishable from the exact results.

Since the mesh points correspond to equal increments in the velocity potential, they are quite dense near the trough of a steep wave and sparse in the vicinity of the crest. For steep capillary waves, therefore, the mesh points cluster in the region of large gradients, which is, overall, a favourable effect. Computed wave speeds in table 1 have converged to 12 decimal places; the errors are due entirely to the inability of the discrete system to model the continuous system exactly and consequently can be expected to diminish rapidly as N becomes large.

While no closed-form solution has been found for the analogous pure-gravity wave problem, quite accurate solutions have been obtained by calculating the coefficients in Stokes' expansion on a computer and then recasting the resulting high-order polynomials as Padé fractions. Longuet-Higgins (1975) and Cokelet (1977), extending the procedure of Schwartz (1972, 1974), have produced converged solutions for wave heights less than one per cent short of that for the maximum, sharp-crested, wave. The critical value of ϵ is now known to be approximately 0·1411. The numerical procedure using equal increments in the velocity potential is not well suited to the calculation of very steep gravity waves because large curvature, low velocity and sparse point spacing are characteristic of the crest region. With $N = 50$, for example, the computed wave speed is in error by one part in 2000 for a steepness of 0·130, which increases to one part in 200 for $\epsilon = 0{\cdot}135$.

	μ			
ϵ	$N = 50$	$N = 75$	$N = 100$	Cokelet (1977)
0·139886	1·19391	1·19392	1·19392	1·19391
0·140435	1·19333	1·19334	1·19334	1·19329
0·140632	1·19316	1·19317	1·19318	
0·140835	1·19307	1·19308	1·19308	
0·140938	1·193058	1·193066	1·193068	
0·140989	1·193060	1·193073	1·193074	

TABLE 2. Wave speed *versus* wave height for steep gravity waves.

It will be shown below that capillary–gravity waves of large steepness are ultimately 'trough-limited'; consequently the program with equal point spacing has proved to be suitable in the general case. However, by modifying the point spacing in a simple manner, the method can yield accurate results in the neighbourhood of the limiting gravity wave as well. We introduce the new independent variable

$$v = \theta^\gamma, \tag{4.2}$$

where $0 < \gamma \leqslant 1$. The domain of the new variable $[0, \pi^\gamma]$ is then subdivided into N equal intervals, i.e.

$$v_i = \frac{i-1}{N}\pi^\gamma, \quad i = 1, \ldots, N+1,$$

and values of the dependent variables are determined at these points.

Table 2 shows values of the dimensionless phase velocity for $N = 50$, 75 and 100 computed for values of wave steepness close to the maximum. The value of γ is taken as $\frac{1}{3}$; thus many points are concentrated near the wave crest. The first two values of ϵ were selected so as to coincide with the two largest values for which Cokelet (1977) computed the wave speed. The computed values for $N = 100$ would appear to have converged to five places following the decimal for all six values of ϵ. For the two highest values we show one additional figure which may not be correct even for $N = 100$. A trend, however, is indicated: the wave speed assumes a local *minimum* value of about 1·19307 for $\epsilon \cong 0{\cdot}14094$. A previous, presumably global, maximum was found by Longuet-Higgins (1975) at $\epsilon \cong 0{\cdot}1387$.

The procedure used to provide the results in table 2 differed in one significant respect from the method described in § 3. The derivative of the ordinate, in this case dy/dv, was used as the unknown rather than y. This would appear to be an improvement in that it removes the need for a numerical differentiation, requiring instead an additional quadrature. Comparison of the two variants however revealed no differences in either accuracy or speed of convergence; we expect equivalent results for steep gravity waves can be obtained from the original formulation via the substitution (4.2) but this has not yet been verified.

(*b*) *Waves with both gravity and surface tension*

The procedure outlined in the last section was used to obtain converged solutions for various combinations of the two input parameters κ and ϵ. It quickly became apparent that waves of several fundamentally different types were produced. In each case, in

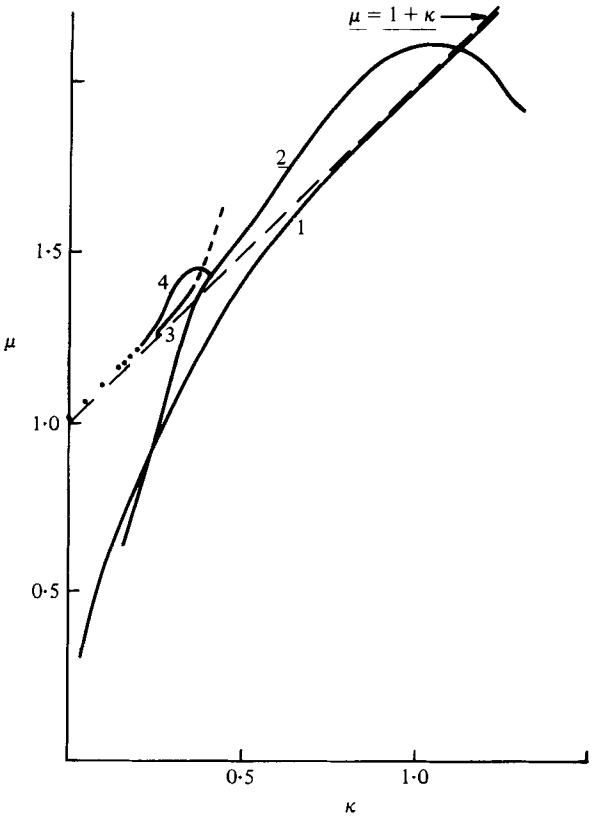

FIGURE 1. Variation of speed parameter μ with capillary number κ for $\epsilon = 0{\cdot}03$.

these preliminary runs, the iteration was started with a simple cosine profile. Once a given solution had been obtained, however, a type of 'boot-strap' technique was employed; that is, a converged solution for one value of κ was used as the initial guess for a wave with κ altered by a few per cent. Similarly, for fixed κ, the amplitude ϵ could be varied using a neighbouring solution as a starting guess. Our objective was to trace the evolution of a wave of given family or type. One computer run, employing this bootstrap method, produced between 10 and 40 converged solutions. The results presented here have been compiled from about 400 solutions. Typically the point parameter N was taken equal to 40; $N = 30$ was adequate for 'easy' profiles and $N = 50$ was used when the converged solutions for smaller values were suspect. A number of consistency checks, for example *a posteriori* computation of the mean water level, were also available.

Figure 1 shows the variation of speed parameter μ with κ for $\epsilon = 0{\cdot}03$. Four continuous families of solutions are displayed, each one labelled with a 'type number'. The type number is, for the most part, indicative of the number of 'dimples' or inflexion points on a (half) wave profile. For much of the figure, the type number is seen to increase with μ for given κ. Also shown is the well-known infinitesimal wave solution

$$\mu = 1 + \kappa.$$

We will refer to this figure several times in the following.

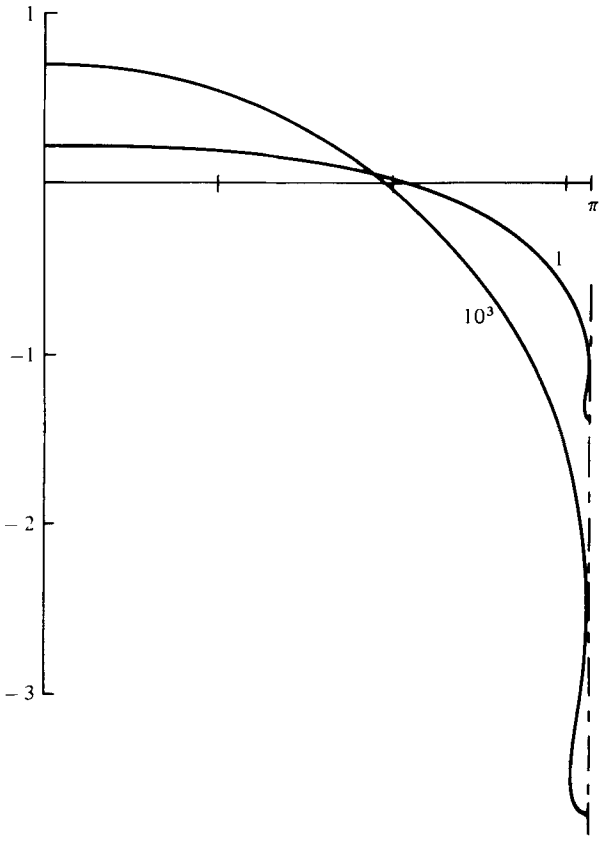

FIGURE 2. Limiting profiles for type 1 waves for $\kappa = 1$ and $\kappa = 1000$.

κ	ϵ	μ	λ_{water} (cm)
∞	0·730	∞	0
10^3	0·727	658·0	0·05
10^2	0·703	66·1	0·17
10	0·556	6·97	0·55
2	0·349	1·69	1·22
1	0·257	1·02	1·73
0·6	0·198	0·74	2·23
0·5	0·179	0·66	2·44
0·43	0·165	0·60	2·63
0·33	0·14	0·4	3·00

TABLE 3. Characteristics of limiting waves of type 1.

The velocity distribution curve labelled type 1 follows the linear solution closely as κ approaches infinity. For this small value of steepness the free-surface profile is indistinguishable from a sinusoid past about $\kappa = 1$. Type 1 is, in fact, the family to which Crapper's pure capillary wave belongs. For relatively large values of steepness, topologically limited waves occur with trapped air bubbles. Figure 2 shows two such profiles for $\kappa = 10^3$ and $\kappa = 1$. For the larger κ, the profile is almost identical to

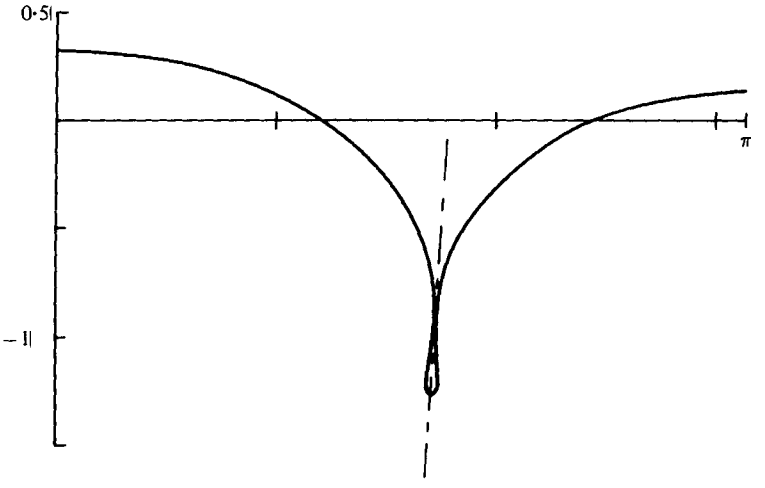

FIGURE 3. A limiting profile for a type 2 wave, $\kappa = 1{\cdot}31$, $\epsilon = 0{\cdot}03$.

Crapper's; the steepness ϵ is equal to 0·727, just 0·4 per cent less than his result. A similar shape is apparent for the limiting profile with $\kappa = 1$. The steepness is much reduced however and the surface is sensibly flat over a substantial portion of the wave.

Table 3 shows limiting values of ϵ and the corresponding values of μ for various κ. Gradients become larger as κ is reduced for these limiting waves; consequently the results for the smallest κ in the table are subject to some uncertainty. For convenience, the equivalent wavelength in water for each value of κ is also given, assuming a value of 74 g s^{-2} for the capillary constant.

The speed curve for the type 2 wave in figure 1 terminates at $\kappa = 1{\cdot}31$. The type 2 waves are characterized, in general, by a secondary maximum on the surface profile with a trough between the two maxima. These troughs may also become deep and narrow; in fact the maximum steepness of type 2 waves is also limited by the entrapment of bubbles. For $\epsilon = 0{\cdot}03$, the value $\kappa = 1{\cdot}31$ is an example of such a limiting case. The profile is shown in figure 3. Note that the true wave steepness greatly exceeds 0·03; the difference between the highest and lowest ordinates divided by the wave length is 0·254, rather close to the limiting steepness of the type 1 wave for this value of κ. Of course, because of the symmetry of the profile about either $x = 0$ or $x = \pi$, each full wavelength will contain two trapped bubbles.

An interesting feature of the wave form in figure 3 is that the trapped bubble is not quite vertical. The centre-line of the bubble, defined as passing through the lowest point and the osculation point, is inclined a bit over 3 degrees from the vertical direction. This centre-line is almost perpendicular to a straight line drawn between the crests at $x = 0$ and $x = \pi$.

Special attention has been paid to those critical values of κ for which Wilton's expansion in powers of ϵ say, and employing Stokes' hypothesis, fails to exist. These are often referred to as the 'resonant cases' since, at these values, according to the linear theory at least, two waves whose lengths are in rational ratio propagate with the same phase velocity. This situation occurs for

$$\kappa = 1/n$$

where $n = 2, 3, \ldots$.

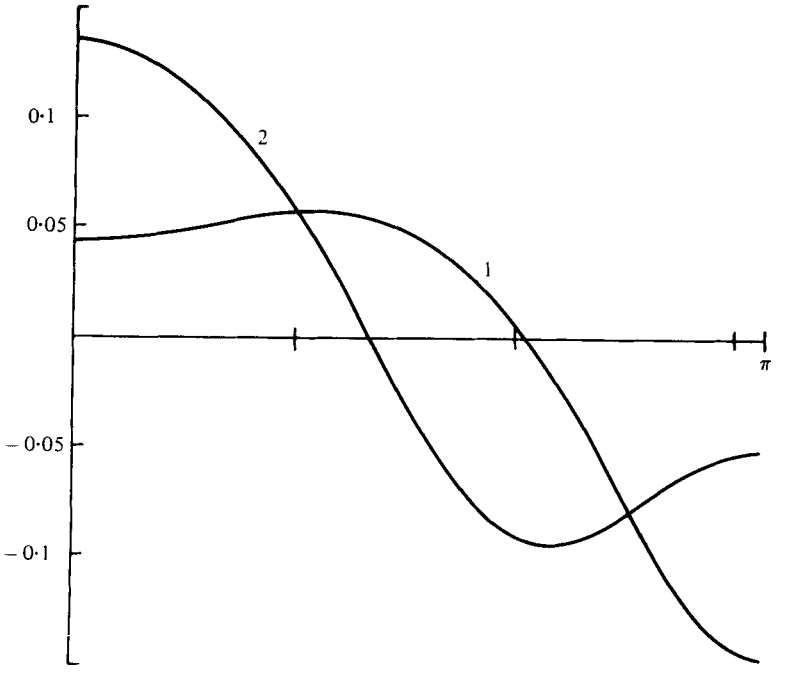

FIGURE 4. Two wave profiles for $\kappa = \frac{1}{2}$ and $\epsilon = 0{\cdot}03$.

Figure 1 reveals that for an established solution of finite amplitude $\kappa = \frac{1}{2}$ is not a special value; for a given ϵ only continuous changes occur in wave form and speed.

The two profiles are shown in figure 4. They are similar to Wilton's third-order solution. The dimples he predicted are confirmed. Note that the vertical scale has been exaggerated by a factor of 10 in this figure. Figure 5 shows a steep wave from each family for $\kappa = \frac{1}{2}$. The type 1 wave is the limiting one and has a trapped bubble at mid-wavelength. Though not discernible in the figure this wave retains a slight crest dimple; the highest point on the profile occurs when x is about 0·7. The type 2 profile was computed for $\epsilon = 0{\cdot}0822$ with $N = 50$. The true steepness of this wave is 0·172, close to the value of ϵ for the other wave. We were unable to compute higher waves of this type for $\kappa = \frac{1}{2}$. We expect the limiting profile to be similar in form to that of figure 3 and exhibit an asymmetric trapped bubble.

The profiles in figures 4 and 5 can also be compared with the predictions of Pierson & Fife (1961). They also find two solutions for $\kappa = \frac{1}{2}$; their 'gravity profiles', our type 2, are similar for small ϵ. Their 'capillary profiles' (type 1) do not have crest dimples, however. This discrepancy may be due to their neglect of higher-order terms.

Figure 6 shows the variation in speed parameter μ with the steepness for the two solutions at $\kappa = \frac{1}{2}$. For the type 1 wave, the speed decreases monotonically with increasing amplitude, as it does for Crapper's exact solution. For small steepness, the speed of the type 2 wave is seen to increase with ϵ; in this respect it is similar to the pure gravity case. A maximum speed is attained however, for $\epsilon \cong 0{\cdot}04$ and the speed falls thereafter as capillary forces become increasingly important. The distinction, therefore, between capillary-dominant and gravity-dominant waves is a bit misleading. We suspect that all waves subject to the combined effects of surface tension

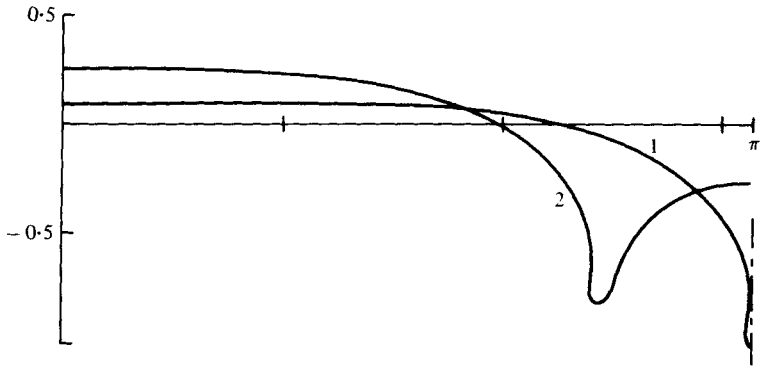

FIGURE 5. Two steep wave profiles for $\kappa = \frac{1}{2}$.

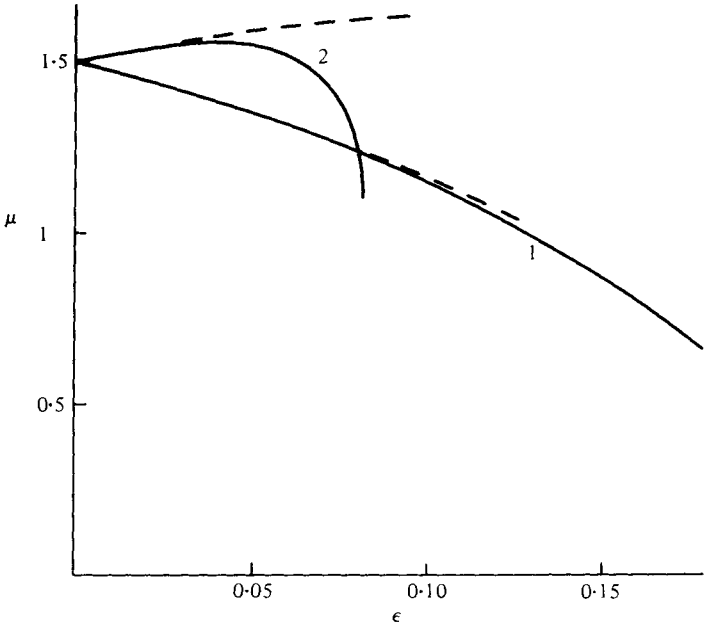

FIGURE 6. Speed parameter μ *versus* ϵ for $\kappa = \frac{1}{2}$;
– – –, 3-term series result of Wilton (1915).

and gravity will *ultimately* become capillary dominant as trough bubbles begin to form.

The dashed lines in figure 6 are Wilton's results. His steepness parameter a, following Stokes (1880), is the amplitude of the first harmonic; it is related to ϵ by

$$\pi\epsilon = a \mp \tfrac{3}{4}a^2 + \ldots. \tag{4.3}$$

Accordingly, his solution becomes

$$\mu = \tfrac{3}{2} \pm \tfrac{3}{4}\pi\epsilon - (\pi\epsilon)^2 + \ldots, \tag{4.4}$$

where the + sign refers to the profile of the second type. One observes that his approximation is quite accurate for the type 1 wave and good for the other wave up to a height of about 0·03. We suspect that each expansion will converge to the corresponding

exact solution when formulated in terms of a suitable, strictly increasing, independent parameter. In fact, the expansions should yield even the highest waves, since these are topologically, rather than singularity, limited.

Many integral properties of capillary gravity waves can be computed from our numerical solution. Perhaps the most important is the energy, which can be divided into kinetic, potential and 'superficial' components. The kinetic and potential energies, as for gravity waves, can be expressed as

$$\mathscr{T} = \frac{\rho c}{2}\int_0^\lambda y\,d\phi \tag{4.5a}$$

and

$$\mathscr{V} = \frac{\rho g}{2}\int_0^\lambda y^2\,dx \tag{4.5b}$$

in terms of dimensional quantities. These are the total respective energies per unit length normal to the plane of the motion for one wave cycle. Derivations of (4.5*a*) and (4.5*b*) may be found in Longuet-Higgins (1975). The superficial energy is simply the product of the capillary constant and the surface extension:

$$\mathscr{S} = T\left[\int_{x=0}^{x=\lambda} ds - \lambda\right], \tag{4.5c}$$

where s is arc length. If we now select as reference energy

$$E_{\mathrm{ref}} = \frac{\rho g \lambda^3}{4\pi^2}$$

and proceed to dimensionless quantities; we obtain the energy coefficients

$$T = -\frac{\mu}{2\pi}\int_0^\pi y\,d\theta, \tag{4.6a}$$

$$V = -\frac{1}{2\pi}\int_0^\pi y^2 x'(\theta)\,d\theta, \tag{4.6b}$$

$$S = \kappa\left[\frac{1}{\pi}\int_0^\pi \sqrt{[x'(\theta)^2 + y'(\theta)^2]}\,d\theta - 1\right]. \tag{4.6c}$$

Note that, in equations (4.6*a*) and (4.6*b*), the surface ordinate y is measured from the mean water level. T and V are the usual energy coefficients, which, to leading order for infinitesimal gravity waves, are each equal to $\frac{1}{4}(\pi\epsilon)^2$.

The dimensionless energies for wave types 1 and 2 and $\kappa = \frac{1}{2}$ are shown in figure 7. There are several notable features. The potential energy reaches a maximum for each family and then decreases with steepness. This is a reflexion of the substantial flattening of much of the free surface as the limiting wave is approached. The kinetic energy generally exceeds the other two, except very near the maximum, where the superficial energy becomes the dominant contribution. The very steep gradients for high waves of the second type indicate that the height parameter employed is probably not the best choice for this case and may explain our failure to obtain the limiting profile. It is clear, however, that type 2 waves are more energetic, partly because they are faster.

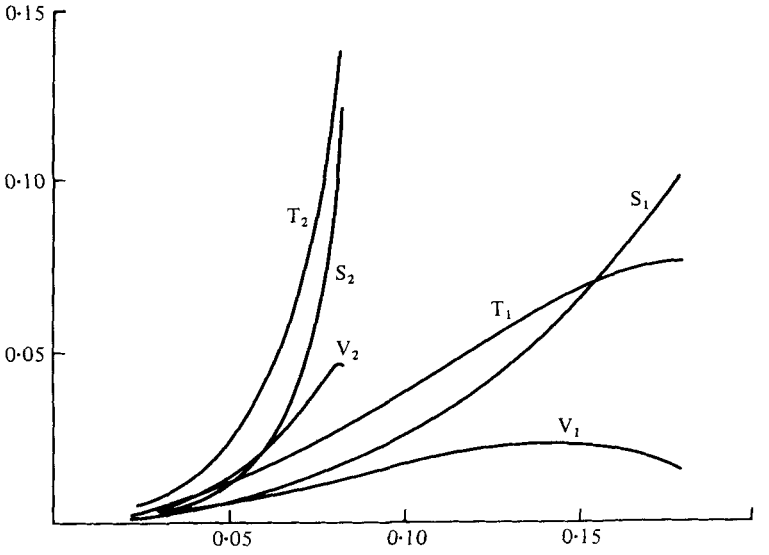

FIGURE 7. Energy coefficients *versus* ϵ for $\kappa = \frac{1}{2}$.

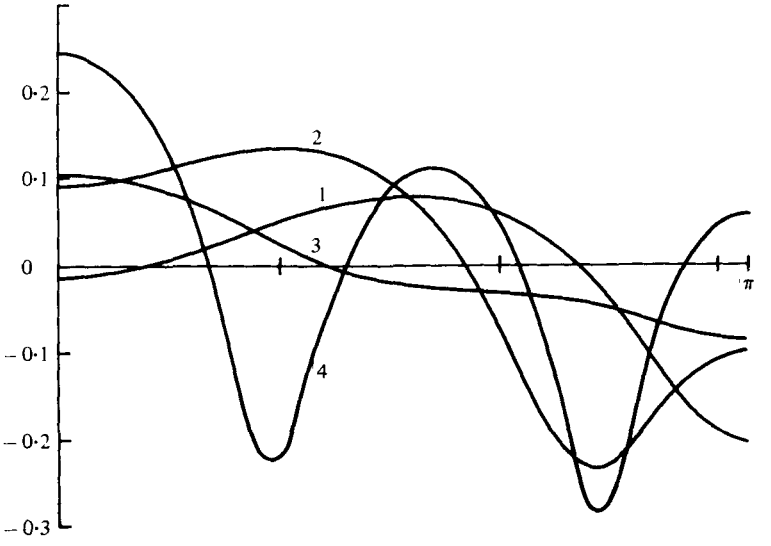

FIGURE 8. Four wave profiles for $\kappa = 0{\cdot}33$ and $\epsilon = 0{\cdot}03$.

Figures 8 and 9 show four wave profiles calculated for $\kappa = 0{\cdot}33$ and $0{\cdot}25$ with $\epsilon = 0{\cdot}03$. The type 1 profiles are similar in shape to the corresponding wave for $\kappa = \frac{1}{2}$ in figure 4. Notice that the crest dimple becomes a bit more pronounced and that the intersection of the profile with the mean water level moves towards the trough as κ is reduced. This latter trend continues as κ is reduced still further and is accompanied by a dramatic fall in speed. The smallest value of κ for which a type 1 solution could be calculated was $0{\cdot}04$ corresponding to a wavelength in water of about 9 cm. The wave speed, from figure 1, can be seen to be about one quarter of that predicted by the linear theory. The wave profile for this case is almost exactly flat for about

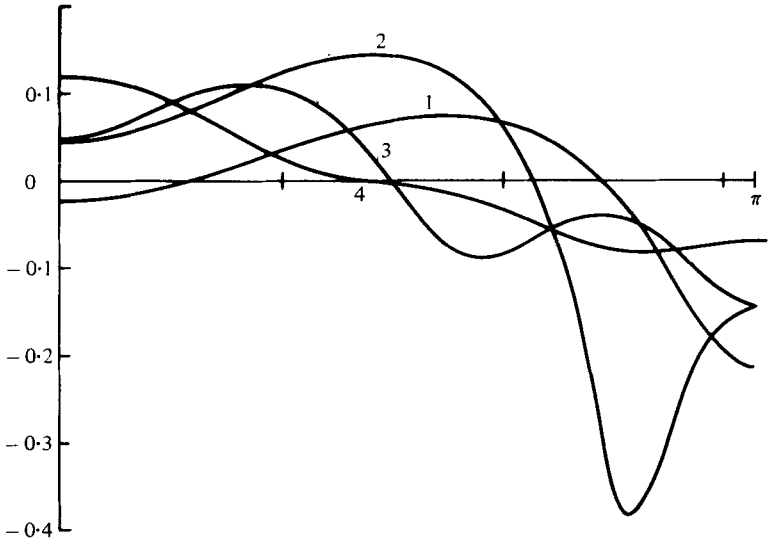

FIGURE 9. Four wave profiles for $\kappa = 0{\cdot}25$ and $\epsilon = 0{\cdot}03$.

κ	Type	I	μ	T	V	S
0·50	1	2	1·4180	0·00434	0·00230	0·00213
0·50	2	2	1·5528	0·00634	0·00356	0·00272
0·33	1	2	1·0976	0·00672	0·00306	0·00389
0·33	2	3	1·2503	0·01666	0·00864	0·00853
0·33	3	3	1·3604	0·00256	0·00170	0·00083
0·33	4	4	1·4297	0·05799	0·01051	0·05016
0·25	1	2	0·9291	0·00599	0·00280	0·00347
0·25	2	3	0·9582	0·02930	0·01280	0·01947
0·2515	3	4	1·2478	0·00646	0·00320	0·00328
0·25	4	4	1·2764	0·00298	0·00217	0·00078

TABLE 4. Wave characteristics for three values of κ, $\epsilon = 0{\cdot}03$.

three-quarters of the wavelength followed by an abrupt hump and an even sharper trough. Figure 1 indicates that the extrapolation $\mu \to 0$ as $\kappa \to 0$ is a reasonable conjecture for the type 1 wave.

The type 2 wave evolves smoothly from the profile shown in figure 4. Note that an additional dimple has appeared at its crest. Also, as κ decreases from 0·33 to 0·25, the trough becomes deeper and narrower. Referring again to figure 1, we see that the speed decreases almost linearly when κ is less than about 0·37. The speed curve for the type 2 wave can also reasonably be extrapolated to the origin.

Figures 8 and 9 show two additional solutions; these have been labelled as types 3 and 4. Notice that for $\kappa = 0{\cdot}33$, the type 3 wave has the appearance of a primary sine wave with a relatively small 3-cycle perturbation superimposed upon it. Similarly at $\kappa = 0{\cdot}25$, the type 4 wave would appear to be a perturbed sinusoid. On the other hand, when they are removed from their 'natural' domains, i.e. type 4 away from $\kappa = 0{\cdot}25$ or type 3 away from 0·33, the high-frequency component is greatly amplified. Referring again to figure 1, we see that, when the ripples are small, the relevant speed

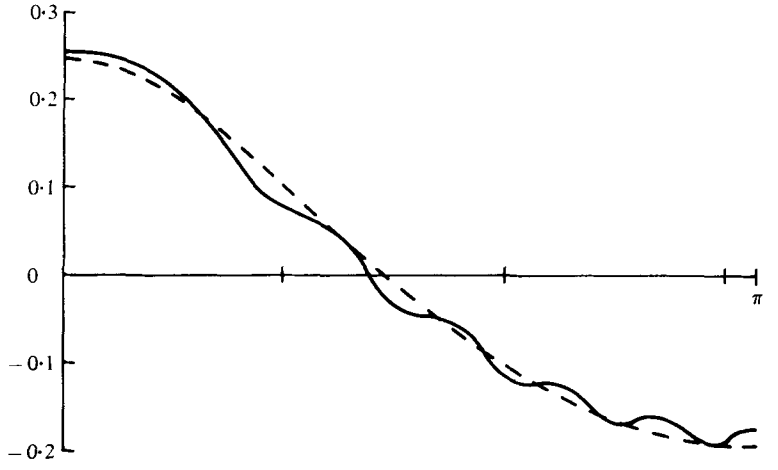

FIGURE 10. Comparison of gravity-dominant wave form with pure gravity wave; ——, $\kappa = 0{\cdot}1$, $\epsilon = 0{\cdot}068$; – – –, $\kappa = 0$, $\epsilon = 0{\cdot}070$.

curve is nearly parallel to the linear solution. On the dashed extension of curve 3 in figure 1, starting at about $\kappa = 0{\cdot}37$, the primary sinusoid has disappeared and the wave form has degenerated to three cycles of the type 1 profile. The lowest value of κ for which the type 3 profile could be computed was 0·2515 with $\epsilon = 0{\cdot}03$. It is this wave that is shown in figure 9. The type 4 wave could be calculated in the range $0{\cdot}21 \leqslant \kappa \leqslant 0{\cdot}41$. For $\kappa = 0{\cdot}20$ a fifth type of wave appeared having one additional inflexion point. Its speed is shown as an isolated point in figure 1. At the other extreme, near $\kappa = 0{\cdot}41$, the type 4 wave exhibits two deep and narrow troughs and appears to be close to the trapped bubble configuration.

Table 4 shows computed values of the parameters for the waves shown in figures 4, 8 and 9. In addition to the speed and energy parameters we give I – the number of inflexion points in the half-wave profile. This would seem to be a somewhat more precise characterization than trying to define what is meant by a dimple.

For $\kappa = \frac{1}{3}$, the perturbation method used by Nayfeh (1970) yielded three solutions, one with three inflexion points and two with five each. None of his three can be compared closely with any of the profiles shown in figure 8, however.

An additional word of explanation is in order concerning the unconnected points lying above the linear solution line in figure 1. All these points represent converged solutions that, except for the gravity wave $\kappa = 0$, have higher-frequency oscillations superimposed upon them. Our experience with the four wave families discussed above leads us to believe that they do not lie on a continuous curve but rather are points selected from a large, indeed infinite, number of continuous curves. As a representative sample we present figure 10 which shows a surface profile with 10 inflexion points for $\kappa = 0{\cdot}10$. The wave height parameter is 0·068, this larger value having been selected so as to more clearly illustrate the surface undulations. For comparison, we show the corresponding pure gravity wave. A physical interpretation would seem clear. The capillary ripples 'ride' on the dominant gravity wave with wavelength appropriate to the local fluid velocity. Thus the faster and shorter ripples appear at the trough. The ripple amplitude, on the other hand, is almost constant and is about

5 per cent of the gravity-wave peak-to-trough height. Note that $\kappa = 0{\cdot}10$ corresponds to a wavelength in water of 5·4 cm.

5. Further remarks

The numerical method of solution employed here, the boundary-integral formulation coupled with Newtonian iteration, would appear to be satisfactory for the solution of two-dimensional free-surface problems with simple flow geometries. In the present work, strong evidence for the *mathematical* existence of capillary–gravity waves of permanent form, even at the resonant wavelengths, has been supplied. Their *physical* existence, on the other hand, involves stability and resonant interaction considerations. For large κ, viscous effects would also be important.

Experimental evidence to date does not seem to be consistent. McGoldrick (1970*a*, *b*), for example, performs experiments using a wave-maker, and claimed that waves of uniform profile cannot exist at resonant conditions. On the other hand Schooley (1960), has published photographs of short-fetch wind-generated water waves in the region of $\kappa = \frac{1}{2}$. Some of his profiles are remarkably similar to the type 2 wave discussed in § 4. Clearly, further experimental work is indicated.

The present numerical solutions should prove useful in theoretical studies of wave interactions and as a starting point for stability analyses. Workers requiring more detailed results than those presented here should contact the first-named author. Important integral properties of these waves, other than those presented here, can be easily calculated.

Apart from the multiplicity of solutions, a given wave form is characterized by three dimensionless parameters, two of which may be regarded as being independent. The set used here, κ, μ and ϵ, is quite an arbitrary choice. Replacing the speed parameter μ by

$$\mu^{\frac{1}{2}}\kappa^{-\frac{1}{2}} = c/c_0$$

provides a measure of phase speed which is independent of wavelength. The reference velocity

$$c_0 = \left(\frac{gT}{\rho}\right)^{\frac{1}{4}}$$

is constant for a given fluid. For water its value is about 16·4 cm s^{-1}. Similarly κ can be replaced by

$$\kappa^{-\frac{1}{2}} = \lambda/\lambda_0,$$

where

$$\lambda_0 = \left(\frac{\rho g}{4\pi^2 T}\right)^{-\frac{1}{2}},$$

which, for water, is about 1·73 cm. Replotting figure 1 with these new variables, equivalent to the dimensional plots found in elementary texts, reveals the physical extrema for the velocity. For $\epsilon = 0{\cdot}03$, the famous (local) speed minimum for the type 1 wave occurs for $\kappa \approx 0{\cdot}97$, corresponding to a slightly larger wavelength than that predicted by linear theory. The type 2 wave is more interesting; it has a local speed minimum at $\kappa \cong 0{\cdot}53$ and a local maximum at $\kappa \cong 0{\cdot}75$. The curve is quite flat however, these 2 extrema differing by less than one per cent. From figure 1, it can be seen that, in the critical region $0{\cdot}3 < \kappa < 1$, the type 2 wave is between 5 and 10 per cent faster than the type 1.

A much more significant change to the set of parameters would be to replace ϵ by a more representative measure of wave steepness. While ϵ is a satisfactory parameter, in general, for the type 1 wave, it is grossly misleading for steep waves of the second kind, where the true steepness is many times larger. In fact the large energy gradients in figure 7 and our inability to find the limiting wave of type 2 for $\kappa = 0{\cdot}5$ may suggest that ϵ is not a monotonically increasing function of true wave steepness.

Based on our numerical experience, we are prepared to offer a few words of conjecture concerning the convergence of Wilton's series. Aside from the critical values $\kappa = 1/n$, we expect the series solution, using Stokes' hypothesis, to be convergent at least for small finite values of steepness. The choice of wave steepness parameter is important, however, if high waves are sought. The series solution can be expected to converge to the wave of type n when κ lies in the open interval $(1/[n+1], 1/n)$, $n = 1, 2, \ldots$. The corresponding wave profile can be expected to have about $n+1$ actual, or latent, inflexions. This 'natural' solution is the one to which the present method will converge if the iteration is started with a simple cosine profile. We are tempted to say that the natural solutions should be the ones most easily found experimentally, as well. Of course when the order n is very large, the capillary undulations will be almost indiscernible and, in addition, will be increasingly affected by viscosity. In fact the average wavelength of the n ripples is inversely proportional to the primary wavelength.

Wilton's modified series for $\kappa = \frac{1}{2}$ can be expected to converge to the two solutions present there. Similar re-orderings should be possible for the smaller critical values. Away from the critical values, the series can yield only one solution, of course. The fate of the other solutions raises a most interesting question.

This work was supported, in part, by the Australian Research Grants Committee.

REFERENCES

Cokelet, E. D. 1977 *Phil. Trans. Roy. Soc.* A **286**, 183.
Crapper, G. D. 1957 *J. Fluid Mech.* **2**, 532.
Crapper, G. D. 1970 *J. Fluid Mech.* **40**, 149.
Harrison, W. J. 1909 *Proc. Lond. Math. Soc.* (2) **7**, 107.
Kamesvara Rav, J. C. 1920 *Proc. Indian Ass. Cultiv. Sci.* **6**, 175.
Keady, G. & Norbury, J. 1978 *Math. Proc. Camb. Phil. Soc.* **83**, 137.
Kinnersley, W. 1976 *J. Fluid Mech.* **77**, 229.
Krasovskii, Yu. P. 1960 *Dokl. Acad. Nauk S.S.S.R.* **130**, 1237.
Levi-Civita, T. 1925 *Math. Ann.* **93**, 264.
Longuet-Higgins, M. S. 1963 *J. Fluid Mech.* **16**, 138.
Longuet-Higgins, M. S. 1975 *Proc. Roy. Soc.* A **342**, 157.
Longuet-Higgins, M. S. & Fox, M. J. H. 1977 *J. Fluid Mech.* **80**, 721.
Longuet-Higgins, M. S. & Fox, M. J. H. 1978 *J. Fluid Mech.* **85**, 769.
McGoldrick, L. F. 1970*a* *J. Fluid Mech.* **40**, 251.
McGoldrick, L. F. 1970*b* *J. Fluid Mech.* **42**, 193.
Nayfeh, A. H. 1970 *Phys. Fluids* **13**, 545.
Nayfeh, A. H. 1971 *J. Fluid Mech.* **48**, 385.
Nekrasov, A. I. 1921 *Izv. Ivanovo-Voznesensk. Politekhn. Inst.* **3**, 52.
Pierson, W. J. & Fife, P. 1961 *J. Geophys. Res.* **66**, 163.
Sasaki, K. & Murakami, T. 1973 *J. Ocean. Soc. Japan* **29**, 94.

SCHOOLEY, A. H. 1960 *J. Geophys. Res.* **65**, 4075.

SCHWARTZ, L. W. 1972 Analytic continuation of Stokes' expansion for gravity waves. Ph.D. dissertation, Stanford University.

SCHWARTZ, L. W. 1974 *J. Fluid Mech.* **62**, 553.

STOKES, G. G. 1849 *Trans. Camb. Phil. Soc.* **8**, 441.

STOKES, G. G. 1880 *Mathematical and Physical Papers*, vol. 1, p. 314. Cambridge University Press.

TRICOMI, F. G. 1957 *Integral Equations*. Interscience.

VANDEN-BROECK, J.-M., SCHWARTZ, L. W. & TUCK, E. O. 1978 *Proc. Roy. Soc.* A **361**, 207.

VAN DYKE, M. 1970 *J. Fluid Mech.* **44**, 365.

WEHAUSEN, J. V. & LAITONE, E. V. 1960 *Handbuch der Physik*, vol. 9 (ed. S. Flügge), p. 446. Springer.

WILTON, J. R. 1915 *Phil. Mag.* **29**, 688.

YAMADA, H. & SHIOTANI, T. 1968 *Bull. Disas. Prev. Res. Inst., Kyoto University*, **18** (135), 1.